Available online at www.sciencedirect.com
ScienceDirect
Earth and Planetary Science Letters 250 (2006) 281 – 291
EPSL
www.elsevier.com/locate/epsl

Timing of Late Pliocene to Middle Pleistocene tectonic events in Rhodes (Greece) inferred from magneto-biostratigraphy and $^{40}Ar/^{39}Ar$ dating of a volcaniclastic layer

Jean-Jacques Cornée [a,*], Philippe Münch [b], Frédéric Quillévéré [a], Pierre Moissette [a], Iuliana Vasiliev [c], Wout Krijgsman [c], Chrystèle Verati [d], Christophe Lécuyer [a,e]

[a] *UMR CNRS 5125 Paléoenvironnements and Paléobiosphère, Université Claude Bernard Lyon I, 27 Bd du 11 Novembre 1918, 69622 Villeurbanne Cedex, France*
[b] *FRE 2761 Géologie des Systèmes Carbonatés, Université de Provence, case 67, 3 place Victor Hugo, 13331 Marseille Cedex 3, France*
[c] *Paleomagnetic Laboratory 'Fort Hoofddijk' Faculty of Earth Sciences, Utrecht University Budapestlaan 17, 3584 CD Utrecht, The Netherlands*
[d] *UMR 6526 Geosciences Azur, Université de Nice Sophia-Antipolis, Parc Valrose, 06108 Nice Cedex 2, France*
[e] *Institut Universitaire de France, France*

Received 15 March 2006; received in revised form 18 July 2006; accepted 24 July 2006
Available online 7 September 2006
Editor: R.D. van der Hilst

Abstract

We discovered a volcaniclastic layer in the Plio-Pleistocene coastal sequences on the island of Rhodes (Aegean fore-arc, Greece). Here, we present an integrated isotopic, magnetostratigraphic, and biostratigraphic (planktonic foraminifers) study for the Haraki section, where this layer is found intercalated in several meters of sedimentary rocks corresponding to the Lindos Bay clay Member of the Rhodes Formation. $^{40}Ar/^{39}Ar$ dating of the volcaniclastic layer provides an age of 1.89±0.09 Ma, which is consistent with our planktonic foraminiferal data. Magnetostratigraphic results show that the entire Haraki section is of normal polarity and according to the isotopic results this corresponds to the Olduvai subchron (1.95–1.77 Ma). The new age determination provides severe constraints for deciphering the sedimentary and tectonic evolution of Rhodes since the Late Pliocene, which can be summarized in the following: (1) 500 to 600 m drowning during the latest Pliocene that could be related to the westward motion of the Anatolian Plate; (2) at least 520 m of uplift at around 1.4–1.3 Ma related to activity of the sinistral strike-slip of the Pliny Trench, the deep Rhodes basin being separated from the island of Rhodes; (3) a counterclockwise rotation of Rhodes, younger than 1.2–1.1 Ma, and possibly synchronous with the young clockwise rotation of the western Aegean arc.

Keywords: $^{40}Ar/^{39}Ar$ dating; Pliocene; Pleistocene; Rhodes; Greece; Mediterranean Sea

1. Introduction

The island of Rhodes (Greece), located in the easternmost part of the Hellenic sedimentary fore-arc, resulted from the Cenozoic subduction of the African Plate beneath the Aegean-Anatolian Plate (Fig. 1). During the Pliocene, westward lateral motion of the Aegean-

* Corresponding author. Tel.: +33 4 78 44 58 21; fax: +33 4 72 44 83 82.
E-mail address: jean-jacques.cornee@univ-lyon1.fr (J.-J. Cornée).

0012-821X/$ - see front matter © 2006 Elsevier B.V. All rights reserved.
doi:10.1016/j.epsl.2006.07.045

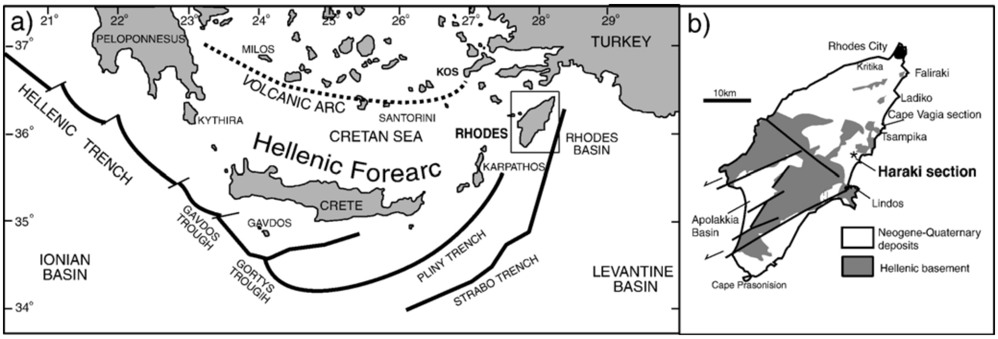

Fig. 1. (a) Location of Rhodes in the eastern Mediterranean; (b) location of the Haraki section.

Anatolian Plate resulted from Arabian-Eurasian plate collision and the Aegean Sea started to collapse (e.g. [1,2]). Rhodes was then exposed to tectonics controlled by N70° trending sinistral strike-slip faults because of the increasing curvature of the plate boundary [3]. Previous studies suggest in addition that Rhodes underwent a counterclockwise rotation phase after 1.8 Ma [4] and some important vertical motions between 2.0 and 1.4 Ma [5]. Vertical movements are still active today (e.g. [6–8]). Despite recent efforts by Cornée et al. [5] (Fig. 2), the chronostratigraphy of the Late Pliocene–Middle Pleistocene deposits of northeastern Rhodes is still poorly understood, mainly because of a lack of absolute age controls. In particular, the exact timing of the young tectonic events is mostly unknown. In this study, a previously unrecognized volcaniclastic layer is described and analyzed. Discrepancies between recently formulated chronostratigraphies can now be resolved on the basis of new, high-precision isotopic ages, combined with magnetostratigraphic and biostratigraphic data. Altogether, these data shed new light upon the young tectonic history of Rhodes, with vertical motion of this part of the fore-arc and rotation of the eastern Aegean arc.

2. Geological setting and stratigraphy

The northeastern part of Rhodes consists of transgressive Pliocene–Pleistocene sediments resting upon a deformed and deeply eroded, mainly calcareous, Mesozoic basement [9,10]. This basement has been faulted, yielding a series of horsts and grabens that later conditioned the nature and distribution of the Pliocene–Pleistocene coastal deposits [11]. Consequently, sedimentary facies changes are common, datings are poorly constrained and correlations between separated graben infillings are difficult to establish.

General stratigraphic studies were conducted by Mutti et al. [10], Meulenkamp et al. [12], Hanken et al. [11] and recently by Cornée et al. [5]. The last authors underlined the uncertainties for dating the sedimentary units from which a recent and rapid tectonic evolution can be discussed. They proposed three lithostratigraphic formations separated by major erosional unconformities: the Rhodes Formation, composed of four Members, the Ladiko-Tsampika Formation, composed of two Members, and the Lindos-Acropolis Formation (Fig. 2). In the

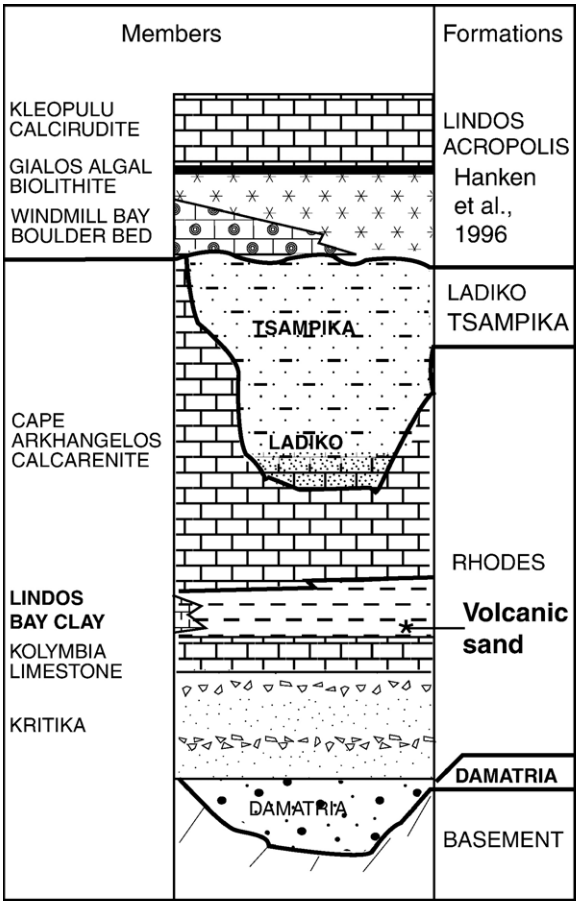

Fig. 2. Sedimentary organisation of the Pliocene–Pleistocene deposits of northeastern Rhodes (from Cornée et al. [5]).

Rhodes Formation, the *Kritika Member* [10–17] is considered either as Late Pliocene [18,19], or latest Pliocene–Early Pleistocene [20], or Early Pleistocene only [21,22]. The *Kolymbia limestone Member* [11,23–25] was attributed to the Late Pliocene [5,26]. The *Lindos Bay clay Member* [11,27] was considered as Pleistocene [12,28,29], or between 3 and 0.7 Ma [26], or Early Pleistocene (i.e. a time span from 1.6 to 1.0 Ma) [21,22], or Late Pliocene to Early Pleistocene (about 2.09 Ma up to around 1.4 Ma) [5]. The Lindos Bay clay Member indicates a major tectonic drowning of eastern Rhodes [5]. The *Cape Arkhangelos calcarenite Member* [11,25,30] was attributed to the Pleistocene [11], between around 1.3 and 1.4 Ma [5]. The calcarenite was deposited during a major tectonic uplift of Rhodes [5]. The *Ladiko-Tsampika Formation* was deposited in palaeovalleys after a major subaerial erosion [5] (Fig. 2). The deposits of the *Ladiko Member* were considered as Late Pliocene [11,14,31] or Pleistocene around 1.3–1.2 Ma [5]. The *Tsampika Member* was considered as Pleistocene around 1.2–1.3 Ma to 0.3 Ma [5]. The Ladiko-Tsampika Formation is overlain by the littoral *Lindos Acropolis Formation* [11] proposed to be younger than 0.3 Ma [5].

The Haraki section outcrops along the track that connects the main road to Agathi Beach (Fig. 1b) (N36°10.863′–E28°05.355′). It is composed of about 6.5 m of Lindos Bay clay (Fig. 3). Three meters above the base of the outcrop is an unconsolidated centimeter-thick layer of volcaniclastic sediment (sample HAR4) exhibiting very high sand-size crystal enrichment. This crystal-rich volcanic sand, sensu Cas and Wright [32], contains angular green amphibole, plagioclase and biotite with a subordinate muddy matrix. Neither vitric fragments (pumice or glass shard) nor lithic fragments (volcanics or else) can be observed. Such crystal concentration effect is well known in primary pyroclastic processes [32] and may not be related to surface epiclastic process. Indeed, if the crystals had been reworked and then deposited long after eruption, they would have mixed with older detritus. The very high proportion of fresh green hornblende, which is usually restricted to pyroclastic deposits, and feldspar, together with the lack of rock fragments, may rather reflect a syn-eruptive feature of volcanic sands [33]. Thus, the volcaniclastic layer should be considered as juvenile, not reworked. It may result of first a typical physical concentration of

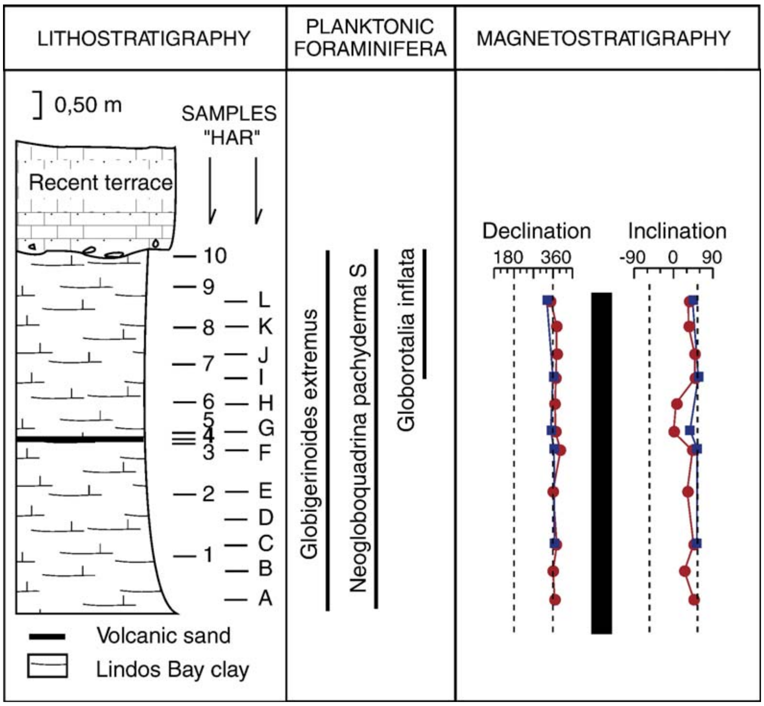

Fig. 3. Lithostratigraphy, planktonic foraminiferal stratigraphy and magnetostratigraphy of the sediments recovered from the Haraki Section. Tick marks show location of samples analyzed for biostratigraphy (labels 1–10) and for magnetostratigraphy (labels A–L). Circles represent the directions obtained from the thermal demagnetization diagrams and squares represent those from the alternating field demagnetization. Both thermal and alternating field demagnetizations provided results interpreted as reliable primary magnetizations. Dashed lines represent declination and inclination of the geocentric axial dipole field for the present latitude of Rhodes Island.

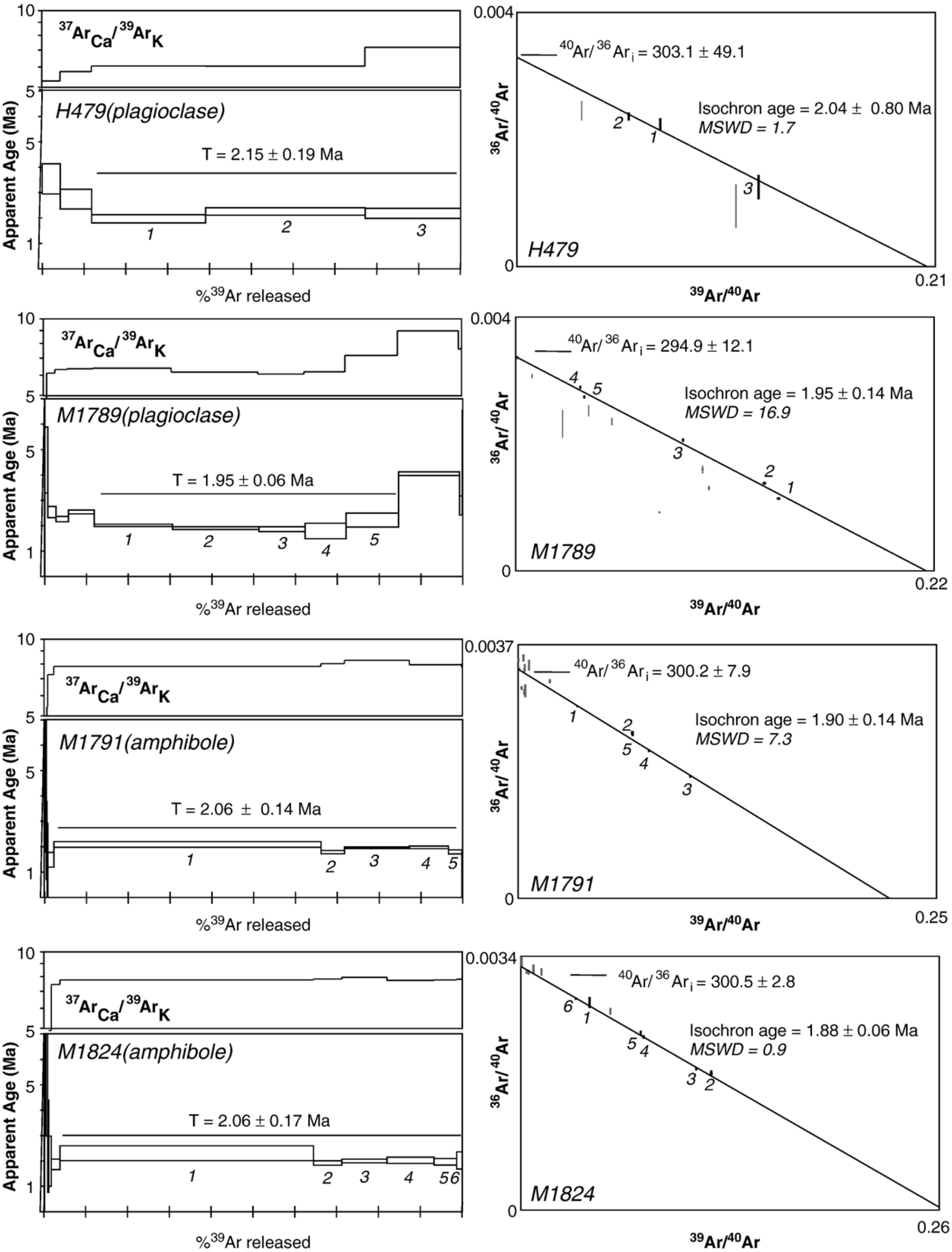

37ArCa/39ArK
H479(plagioclase)
T = 2.15 ± 0.19 Ma
Apparent Age (Ma)
%39Ar released
40Ar/36Ari = 303.1 ± 49.1
Isochron age = 2.04 ± 0.80 Ma
MSWD = 1.7
H479
36Ar/40Ar
39Ar/40Ar
0.004
0.21
37ArCa/39ArK
M1789(plagioclase)
T = 1.95 ± 0.06 Ma
40Ar/36Ari = 294.9 ± 12.1
Isochron age = 1.95 ± 0.14 Ma
MSWD = 16.9
M1789
0.22
37ArCa/39ArK
M1791(amphibole)
T = 2.06 ± 0.14 Ma
40Ar/36Ari = 300.2 ± 7.9
Isochron age = 1.90 ± 0.14 Ma
MSWD = 7.3
M1791
0.0037
0.25
37ArCa/39ArK
M1824(amphibole)
T = 2.06 ± 0.17 Ma
40Ar/36Ari = 300.5 ± 2.8
Isochron age = 1.88 ± 0.06 Ma
MSWD = 0.9
M1824
0.0034
0.26

pyroclastic crystals during an explosive volcanic eruption and, second, a pene-contemporaneous mass flow redeposition in a deep marine environment (400–600 m depth [11,34]). Such syn-eruptive epiclastic transport may account for the preservation of the angular shape of crystals and crystal fragments and could be responsible for deposition through appreciable distances [32]. However, it must be pointed out that no volcanic activity is known on the island of Rhodes after 27.2 Ma [35].

3. Materials and methods

3.1. Ar/Ar dating

Crystals of amphibole and plagioclase were extracted from the sediment and were analyzed by $^{40}Ar/^{39}Ar$ step heating procedure. Their chemical compositions were determined by electron microprobe analyses at the University of Montpellier II, France (Table A in Appendix A). Plagioclases are andesine with composition falling into the range An33.8–An47.5 and with K_2O content between 0.4% and 0.7%. Amphiboles are magnesio-hornblende with Mg# in the range 62.5–67.7 and with K_2O content in the range of 0.6–0.8%. Despite their optically fresh aspect, biotites were not analyzed because they are altered, as revealed by their water content larger than 10% (Mg# in the range of 61.2–62.2).

Samples were crushed and plagioclase and amphibole crystals were concentrated by using standard heavy liquid and/or Frantz magnetic separator. The grain size for the amphibole and plagioclase crystals was in the order of 160–200 μm. The separated crystals were cleaned in 1 N nitric acid to dissolve possible carbonate impurities, then rinsed in successive ultrasonic baths of distilled water and pure alcohol. Finally, the grains were selected under a binocular microscope.

All samples were irradiated for 1 h or 1.2 h in the nuclear reactor at the McMaster University in Hamilton (Canada), in position 5c along with Alder Creek Sanidine (ACs-2) neutron fluence monitor for which an age of 1.193 Ma is adopted and is equivalent to an age for Fish Canyon Sanidine of 28.02 Ma [36]. The estimated error bar on the monitor $^{40}Ar*/^{39}Ar_K$ ratio (directly related to the flux gradient) is ±0.4% (2σ) in the volume where the samples were included. $^{40}Ar/^{39}Ar$ age determinations were performed in the Geosciences Azur laboratory at Nice (France). The step-heating experiments on the amphibole and plagioclase bulk samples (Table B in Appendix A) were performed in a double-vacuum tantalum crucible system heated by a high-frequency furnace, and connected to a stainless steel purification line with two GP50 Al–Zr Getters operating at 400 °C with an ($LN2+Cl_2CH_2$) cold trap. The mass spectrometer is a 120° M.A.S.S.E. flight tube fitted to a Baur-Signer GS-98 source and a Balzers SEV217 electron multiplier. For a small cluster (3 mg) of plagioclase grains, gas extraction was carried out with a continuous Synrad 48-5 CW CO_2 laser beam; the mass spectrometer is a VG 3600 working with a Daly detector system. On the laser line, the gas was purified in stainless and glass extraction line using two Al–Zr getters (working at 400 °C and ambient temperature, respectively) and an LN2 cold trap. The typical total blank values for the extraction and purification laser system are reported in Table C. Mass discrimination for both mass spectrometers was monitored by regularly analyzing one air pipette volume (Table C in Appendix A). The criteria for defining plateau ages are: (1) plateau steps should contain at least 70% of released ^{39}Ar, (2) there should be at least three successive steps in the plateau and (3) the integrated age of the plateau should agree with each apparent age of the plateau within a 2σ confidence interval. All the subsequent quoted uncertainties are thus at the 2σ level.

3.2. Palaeomagnetism

Oriented hand samples for magnetostratigraphy were taken in the field and were drilled later in Fort Hoofddijk laboratory of Utrecht University using compressed air. To establish the polarity pattern of Haraki section at least one specimen from eleven out of twelve layers (one level failed) was stepwise thermally demagnetized. The demagnetization was performed with small temperature increments of 20–40 °C up to a maximum temperature of 620 °C, in a magnetically shielded, laboratory-built, furnace. The natural remanent magnetization (NRM) was measured on a horizontal 2G Enterprises DC SQUID cryogenic magnetometer (noise level 3×10^{-12} A m^2). Additionally, where existing, a second sample was demagnetized using alternating field demagnetization. The

Fig. 4. $Ar/^{39}Ar$ age spectra, $^{37}Ar_{Ca}/^{39}Ar_K$ spectra and the corresponding inverse isochrons. All errors are quoted at 2σ level (plateau and isochron ages, initial intercept). The uncertainties on the $^{40}Ar/^{39}Ar$ ratios of the fluence monitors (0.4% at 2σ) are included in the calculation of the plateau age uncertainties, but the error on the age of the monitor is not included in the calculation. Uncertainties on the apparent ages on each step are quoted at the 1σ level. In the inverse isochron diagram, the data in grey colour are the steps not considered for the plateau age nor for the isochron age. For each dating, isochron data and the corresponding steps of the age plateau have the same number (1 to 6). MSWD=mean square of weighted deviates.

demagnetization steps were: 0, 3, 5, 8, 10, 15, 20, 25, 30, 25, 40, 50, 60, 70, 80, 90, 100 mT. The NRM for the alternating field demagnetized samples was measured using an in-house built robotized sample handler controller, attached to a horizontal 2G Enterprises DC SQUID cryogenic magnetometer. The directions of the NRM components were calculated by principal-component analysis [37].

Furthermore, several rock-magnetic experiments were performed to identify the carriers of the magnetization. Thermomagnetic measurements were performed in air up to 700 °C for 2 powdered samples from diverse lithologies on a modified horizontal translation type Curie balance (noise level 5×10^{-9} A m^2) [38]. Hysteresis loops were measured for 2 samples on an alternating gradient magnetometer (MicroMag Model, Princeton, noise level 2×10^{-8} A m^2) to determine the saturation magnetization (M_s), remanent saturation (M_{sr}), coercive force (B_c) and remanent coercivity (B_{cr}). First order reversal curves (FORC) [39,40] were measured for 2 samples to evaluate the magnetic domain situation, the presence of magnetic interactions and the magnetic mineralogy. For each FORC diagram, 200 curves were measured with an average time of 0.2 s per data point.

3.3. Planktonic foraminiferal analysis

Our planktonic foraminiferal analysis is based on the study of 10 samples (~ 0.7 m spacing), collected between the base and the top of the Lindos Bay clay recovered in the Haraki section. Sample spacing was lower (~ 0.1 m) in the vicinity of the volcanic sand (Fig. 3). Samples were washed over a 65 μm screen. The residue was dry-sieved and the size fractions coarser than 125 μm were used for further investigations. About 1500 specimens were picked under a binocular microscope and identified following the taxonomic concepts and nomenclature of Kennett and Srinivasan [41].

4. Results

4.1. $^{40}Ar/^{39}Ar$ geochronology

The plagioclase bulk sample (#m1789) displays a plateau age of 1.95 ± 0.06 Ma (corresponding to 72.7% of ^{39}Ar released) whereas it gives a saddle-shaped age spectrum characterized by disturbed apparent ages, around 4 Ma, at very low temperature and at highest temperatures (Fig. 4). The inverse isochron ($^{36}Ar/^{40}Ar$ vs. $^{39}Ar_K/^{40}Ar$) for the five plateau steps only yields an age of

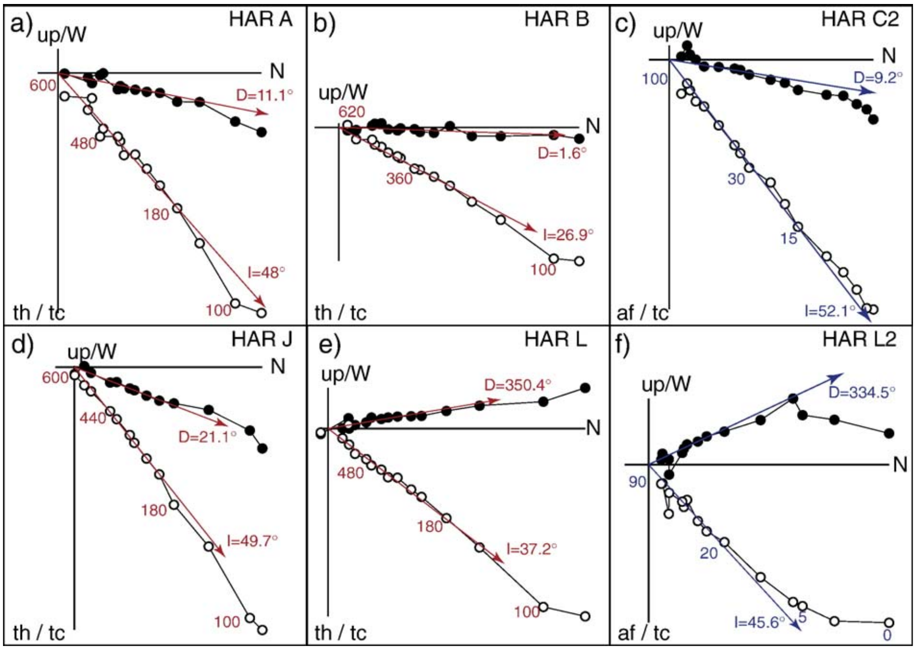

Fig. 5. Orthogonal projections of stepwise thermal (th) and alternating field (af) demagnetization (Zijderveld) diagrams of samples from the Haraki section. The sample codes are in the upper right corner. Solid (open) circles represent the projection of the ChRM vector-end point on the horizontal (vertical) plane. Numbers indicate temperature (th) or magnetic field (af) steps in °C or respectively mT. The diagrams are represented with tectonic corrections (tc). The arrows indicate the interpreted ChRM directions, D, declinations and I, inclinations.

1.95±0.14 Ma (initial atmospheric $^{40}Ar/^{36}Ar$ ratio of 294.9±12.1, MSWD=16.9, Fig. 4). The initial $^{40}Ar/^{36}Ar$ ratio value is indistinguishable from that of air (295.5) indicating that no extraneous argon is considered in the calculated ages. The laser experiment of a small cluster of transparent plagioclase crystals (#h479) displays a plateau age of 2.15±0.19 Ma (corresponding to 88.13% of ^{39}Ar released). The inverse isochron for the three plateau steps gives an age of 2.04±0.80 Ma (initial atmospheric $^{40}Ar/^{36}Ar$ ratio of 303.1±49.7, MSWD=1.73, Fig. 4). The age obtained by laser experiment is slightly older than the one obtained in the furnace but still concordant. This is the result of the small number of steps not allowing to distinguish at the highest temperatures the argon excess observed in the furnace experiment. Thus, this age includes an excess argon component as shown by the slightly higher initial atmospheric $^{40}Ar/^{36}Ar$ ratio.

Both amphibole bulk samples (#m1791 and m1824) display similar plateau ages of 2.06±0.14 Ma and 2.06±0.17 Ma, corresponding to 97.5% and 96.1% of ^{39}Ar released, respectively. The inverse isochron ages, calculated only for the plateau steps, are slightly younger but concordant with the plateau ages: the experiment #m1791 provides an age of 1.90±0.14 Ma (initial atmospheric $^{40}Ar/^{36}Ar$ ratio of 300.2±7.9, MSWD=7.3, Fig. 4) and the experiment #m1824 provides an age of 1.88±0.06 Ma (initial atmospheric $^{40}Ar/^{36}Ar$ ratio of 300.5±2.8, MSWD=0.9, Fig. 4).

All measured ages are concordant at the 2σ level showing that the amphibole and plagioclase crystals belong to the same eruption or cycle of eruptions. This confirms that the crystal-rich volcanic sand is not reworked by surface epiclastic process but is mainly related to pyroclastic processes. The weighted mean age of the four concordant isochron ages is 1.89±0.09 Ma (2σ) and is retained as the best estimate of the volcaniclastic layer age.

4.2. Rock and palaeomagnetism

The Haraki samples are characterized by high initial intensities of the NRM, in the range of 3–45 mA/m. The susceptibility of the samples decreases continuously, without any visible increase upon heating to the highest temperatures (620 °C) suggesting the presence of an iron oxide as the carrier of the magnetization. The thermal demagnetization diagrams are characterized by linear decay of the NRM to temperatures of 580–620 °C (Fig. 5a, b, d and e). The alternating field demagnetization diagrams show that almost all the magnetization is removed in fields of 90–100 mT (Fig. 5c and f), suggesting a relatively soft, low coercivity component, likely magnetite. The Curie balance measurements (Fig. 6a) reveal that the dominant magnetic carrier for this group of samples is a mineral with a maximum blocking temperature (Tb) in the range of 580–620 °C, close to the Curie temperature (Tc) of magnetite [42]. The FORC diagrams (Fig. 6b) infer an interacting multi-domain (MD) state of the magnetic minerals with a maxima around 15 mT [39,40]. Furthermore, the hysteresis curves, up to fields of 2 mT, are almost closed around 300 mT (Fig. 6c). It confirms the presence of a (dominant) low-coercivity mineral (most likely magnetite) accompanied by a high-coercivity mineral like hematite and/or maghemite.

Based on the results of rock magnetic analyses, we conclude that the main carrier of the demagnetization is a

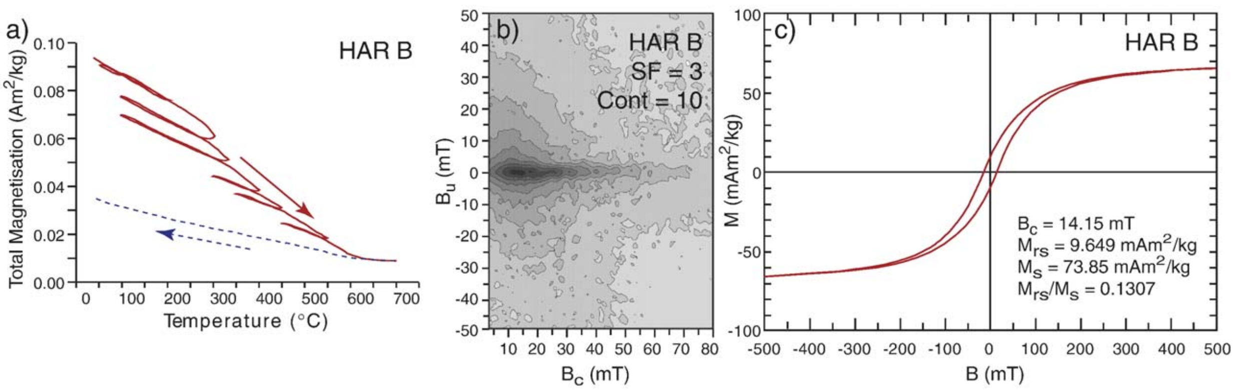

Fig. 6. Rock magnetic measurements for the sample HAR B (considered characteristic for the section). (a) Thermomagnetic runs performed in air on a modified horizontal translation-type Curie balance (noise level 5×10^{-9} A m^2) [38]. Heating (solid line) and cooling (dashed line) were performed with rates of 10 °C/min. The cycling field varied between 150 and 300 mT. (b) Hysteresis curve measured for -2 T $\leq B \leq 2$ T, on an alternating gradient magnetometer (MicroMag Model Princeton, noise level 2×10^{-8} A m^2). In the figure, the results up to ±500 mT are shown, with applied paramagnetic contribution and mass corrections. (c) Representative FORC diagrams. Smoothing factor (SF)=3, 10 contours, MD with low coercivity and peak position ~14 mT.

detrital, multi-domain magnetite. This mineral is known to be a stable, reliable carrier of the magnetization preserving usually a characteristic remanent magnetization ChRM. The magnetization directions can be reliably determined in the demagnetization diagrams and reveal only normal components in the Haraki section, both in the thermally demagnetized samples and after alternating field treatment (Fig. 3). The consistent directions and the results of the rock magnetic analyses warrant the conclusion that the ChRM is the original NRM acquired during deposition. Hence, we can conclude the entire Haraki section must have been deposited during a period of normal polarity of the Earth's magnetic field. Unfortunately, sample orientation and laboratory treatment have not been careful enough to reliably determine the sense of vertical axis rotation from these results.

4.3. Foraminifers

Planktonic foraminifers are abundant in all samples and their preservation ranges from moderate to good. A rich fauna of 24 taxa was thus documented. All samples provided typical specimens of *Globigerinoides extremus*, for which the last appearance datum (LAD) has been calibrated at 1.77 Ma (top of Olduvai subchron) in the Mediterranean region [43–45]. The benthic foraminifer *Hyalinea balthica* was not discovered in any of the 10 samples. Likewise, none contains a significant number of sinistrally coiled specimens of *Neogloboquadrina pachyderma*, which would have indicated an age younger than 1.80 Ma for the Lindos Bay clay recovered in the Haraki section. The top 1.5 m of the section provided in addition numerous specimens of *Globorotalia inflata*, for which the first appearance datum (FAD) has been calibrated at 2.09 Ma (early Matuyama) in the Mediterranean region [43,45,46]. The co-occurrence of *G. extremus* and *G. inflata* suggests that at least the top of the Haraki section was deposited during the 2.09–1.80 Ma time span (Late Pliocene, Olduvai subchron or top of Chron C2r.1r), and corresponds to the upper part of planktonic foraminiferal Zone PL6 of Berggren et al. [43]. The lower part of the section (below the volcaniclastic layer) appears to be biostratigraphically uncertain because of the lack of key species.

5. Discussion

5.1. Integrated chronostratigraphy

The occurrence of pyroclastic fallout at 1.89 ± 0.09 Ma in Rhodes Island is problematic regarding its fore-arc location and the lack of volcanic activity since the Oligocene. However, a Pliocene–Pleistocene volcanic activity is known in the Kos-Nysiros area located less than 100 km northwest of Rhodes (Fig. 1a), at the eastern end of the modern Hellenic volcanic arc [35,47–51]. The volcanic activity in Kos island started during the Pliocene and went on through the Early Pleistocene (3.4–1.0 Ma; K/Ar datings), with calc-alkaline dacitic and rhyolithic domes and rhyolithic phreatomagmatic deposits [49]. Highly porphyritic andesitic lavas were also emplaced in Pachia, Perigusa and in the lower part of the succession in Nisyros island since ~3 Ma according to DiPaola [47]. The mineralogical assemblage of the HAR4 sample in Haraki may correspond to a calc-alkaline andesitic to dacitic composition of the magma that fits the chemistry of the investigated pyroclastic crystals.

In the Haraki section, the $^{40}Ar/^{39}Ar$ age determination of 1.89 ± 0.09 Ma for the volcaniclastic layer is biostratigraphically corroborated by the co-occurrence of *G. extremus* and *G. inflata* in the sediments that rest directly upon it. The normal magnetic polarity identified along the whole section is consequently assigned to the Olduvai subchron (C2n, 1.950–1.770 Ma; [44]) in the astronomically calibrated timescale (APTS). These data suggest therefore a Late Pliocene age for the lower part of the Lindos Bay clay Member, corroborating previous interpretations by Cornée et al. [5]. Consequently:

(1) Under the latest Pliocene Lindos Bay clay, the Kolymbia limestone and the Kritika Members are Late Pliocene in age (presence of *G. inflata* in the Kritika Member: [14,31]);
(2) The Lindos Bay clay Member was deposited between the latest Pliocene (Olduvai subchron in Haraki and Vagia sections) and the Early Pleistocene (around 1.4 Ma, determined from the FCO of *H. balthica* in the Faliraki section [21,22]);
(3) The two normal magnetic polarity intervals in the overlying Ladiko-Tsampika Formation have to be assigned to the Jaramillo and Brunhes subchrons, Early to Middle Pleistocene.

5.2. Timing of tectonic episodes

The Pliocene–Pleistocene deposits of eastern Rhodes recorded tectonic events of short duration (100–200 kyr long), separated by longer low-subsidence periods (400 kyr–1 Ma) (Fig. 7):

(1) In the now confirmed latest Pliocene, between around 2 Ma and around 1.8 Ma, Rhodes was

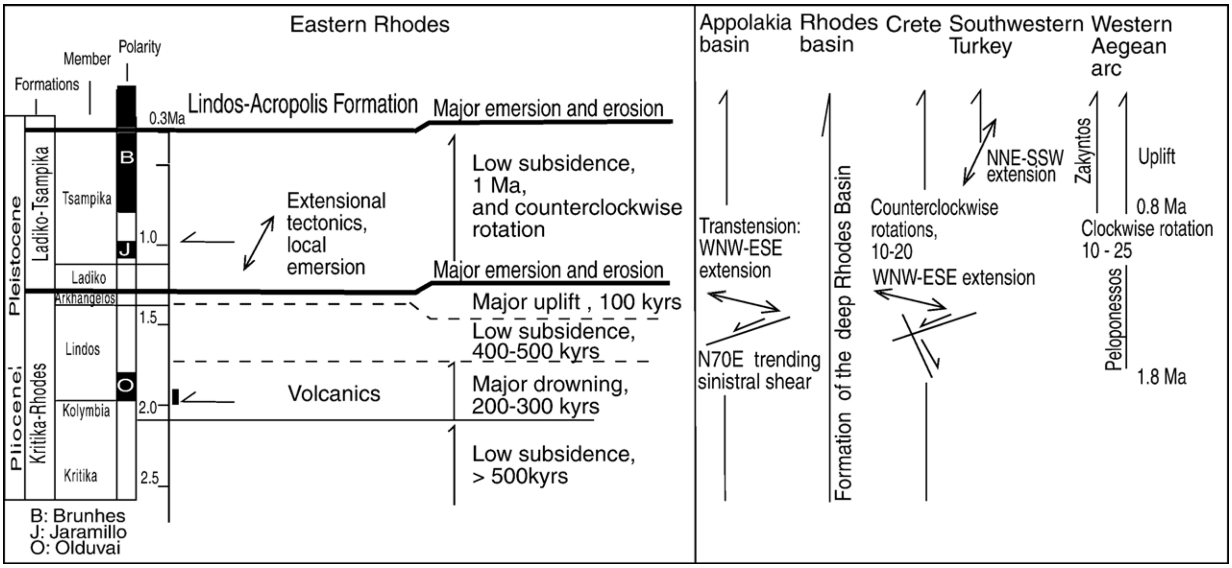

Fig. 7. Late Pliocene–Middle Pleistocene tectonic episodes in eastern Rhodes. Appolakia basin [3]; Rhodes basin [53]; Crete [58]; southwestern Turkey [1]; western Aegean arc [4,54–57].

rapidly drowned during the deposition of the Kolymbia limestone and Lindos Bay clay, with a vertical motion which reached 500 to 600 m [5,34,52];

(2) At around 1.4–1.3 Ma, Rhodes was uplifted during the deposition of the Cape Arkhangelos calcarenite. The vertical motion was at least 520 m [5];

(3) At now confirmed around 1.1–1.0 Ma the Ladiko-Tsampika Formation suffered an extensional tectonic event (TS4 sequence of Cornée et al. [5]).

These tectonic events may be linked to the young tectonic evolution of the Aegean sea:

(1) The important vertical motions during the latest Pliocene and the Early Pleistocene are coeval with the Pliocene–Pleistocene crustal uplift of the Aegean internal arc because of the lateral extrusion of the Anatolian plate since around 3 Ma [1,2]. At this moment, volcanic activity occurred in the eastern Aegean volcanic arc in Kos and Nysiros and the deep Rhodes basin was probably created [53]. Because of the increasing curvature of the fore-arc, Rhodes and the Rhodes basin were then separated at around 1.4–1.3 Ma, probably along the sinistral Pliny-Strabo trench strike-slip zone [3,5] (Fig. 1).

(2) A 10° counterclockwise rotation of the eastern Aegean arc was proposed to occur after 1.8 Ma [4]. In this study, some of the samples from Rhodes were taken from the lower part of the new Ladiko-Tsampika Formation. Consequently, the counterclockwise rotation of Rhodes occurred after around 1.2–1.1 Ma and it is associated with a low subsidence period (around 0.1–0.2 mm/yr [5]). The rotation of Rhodes is not related to major vertical motions, but occurred a short time after (Fig. 7). It may, however, be synchronous with the young clockwise rotation of the western Aegean arc [54–57] which was proposed to begin after 1.8 Ma, in some areas at around 0.8 Ma [4,57];

(3) The sequence TS4 of the Ladiko-Tsampika Formation, now confirmed at around 1 Ma, recorded an extensional tectonic event with faulted blocks and south to southeastward slidings [5]. This extensional event is coeval with the major change in the tectonic regime of the Aegean fore-arc: at around 1 Ma extension in central and northern Greece changed rapidly from NE–SW direction to NNW–SSE direction [4].

6. Conclusion

The age determination of 1.89±0.09 Ma for the volcaniclastic layer analyzed in the lowermost part of the Lindos Bay clay Member, associated with new magnetostratigraphic and biostratigraphic data, allows to calibrate the chronostratigraphy of the Pliocene–Pleistocene deposits of northeastern Rhodes. The Kritika and the Kolymbia limestone Members were clearly deposited during the Late Pliocene. The overlying Lindos Bay clay

Member is dated from the latest Pliocene to the Early Pleistocene at 1.4 Ma. The Cape Arkhangelos calcarenite is Early Pleistocene in age, at approximately 1.4–1.3 Ma. The new Ladiko-Tsampika Formation is dated from around 1.2 Ma to around 0.3 Ma. These ages suggest the following tectonic evolution of Rhodes: (1) 500 to 600 m of drowning during the latest Pliocene that could be related to the Anatolian Plate westward motion; (2) at least 520 m of uplift at around 1.4–1.3 Ma, related to the activity of the sinistral strike-slip of the Pliny and Strabo trenches; when the deep Rhodes basin separated from Rhodes; (3) Rhodes underwent a young counterclockwise rotation, since around 1.2–1.1 Ma, probably synchronous with the young clockwise rotation of the western Aegean arc; (4) an NNW–SSE trending extension is recorded during the deposition of the Ladiko-Tsampika Formation at around 1 Ma, as in central and northern Greece.

Acknowledgements

Financial support was provided by the CNRS (UMR 5125 PEPS) and the Institut Universitaire de France. We acknowledge the help of J.P. Suc, S. Joannin, E. Koskeridou and P. Desvignes who participated in the fieldwork with us.

Appendix A. Supplementary data

Supplementary data associated with this article can be found, in the online version, at doi:10.1016/j.epsl.2006.07.045.

References

[1] C. Facenna, O. Bellier, J. Martinod, C. Piromallo, V. Regard, Slab detachment beneath eastern Anatolia: a possible cause for the formation of the Anatolian fault, Earth Planet. Sci. Lett. 242 (2006) 85–97.

[2] P. Gautier, J.-P. Brun, R. Moriceau, D. Sokoutis, J. Martinod, L. Jolivet, Timing, kinematics and cause of the Aegean extension: a scenario based on comparison with simple analogue experiments, Tectonophysics 315 (1999) 31–72.

[3] J.H. ten Veen, K.L. Kleinspehn, Geodynamics along an increasingly curved convergent plate margin: Late Miocene–Pleistocene Rhodes, Greece, Tectonics 21 (2002) 1–21.

[4] C.E. Duermeijer, M. Nyst, P.T. Meijer, C.G. Langereis, W. Spakman, Neogene evolution of the Aegean Arc; paleomagnetic and geodetic evidence for a rapid and young rotation phase, Earth Planet. Sci. Lett. 176 (2000) 509–525.

[5] J.J. Cornée, P. Moissette, S. Joannin, J.P. Suc, F. Quillévéré, W. Krijgsman, F. Hilgen, E. Koskeridou, P. Münch, C. Lécuyer, P. Desvignes, Tectonic and climatic controls on coastal sedimentation: the Late Pliocene–Middle Pleistocene of northeastern Rhodes, Greece, Sediment. Geol. 187 (2006) 159–181.

[6] P.A. Pirazzoli, L.F. Montaggioni, J.F. Saliege, G. Segonzac, Y. Thommeret, C. Vergnaud-Grazzini, Crustal block movements from Holocene shorelines: Rhodes Island (Greece), Tectonophysics 170 (1989) 89–114.

[7] P.A. Pirazzoli, L.F. Montaggioni, J. Thommeret, V. Thommeret, J. Laborel, Sur les lignes de rivage et la néotectonique à Rhodes (Grèce) à l'Holocène, Ann. Inst. Oceanogr. 58 (1982) 89–102.

[8] N.C. Flemming, P.L. Woodworth, Monthly mean sea levels in Greece during 1969–1983 compared to relative vertical land movements measured over different timescales, Tectonophysics 148 (1988) 59–72.

[9] E. Lekkas, G. Danamos, E. Skourtsos, D. Sakellariou, Position of the Middle Triassic Tyros beds in the Gavrovo-Tripolis unit (Rhodes island, Dodecanese, Greece), Geol. Carpath. 53 (2001) 37–44.

[10] E. Mutti, G. Orombelli, R. Pozzi, Geological studies on the Dodecanese Islands (Aegean Sea). IX. Geological map of the island of Rhodes (Greece); explanatory notes, Ann. Geol. Pays Hell. 22 (1970) 79–226.

[11] N.-M. Hanken, R.G. Bromley, J. Miller, Plio-Pleistocene sedimentation in coastal grabens, north-east Rhodes, Greece, Geol. J. 31 (1996) 271–296.

[12] J.E. Meulenkamp, E.F.J. De Mulder, A. Van De Weerd, Sedimentary history and paleogeography of the Late Cenozoic of the Island of Rhodos, Z. Dtsch. Geol. Ges. 123 (1972) 541–553.

[13] J.A. Broekman, Sedimentary structures and paleoecology of the Pliocene Kritika Formation in a section near Kalithies (Rhodos, Greece), Proc. K. Ned. Akad. Wet., B 76 (1973) 423–445.

[14] J.A. Broekman, Sedimentation and paleoecology of Pliocene lagoonal-shallow marine deposits on the Island of Rhodes (Greece), Utrecht Micropaleontol. Bull. 8 (1974) 1–142.

[15] S. Benali-Baitich, Paléobiocoenoses d'ostracodes dans les coupes Faliraki I et II de la Formation de Kritika (Pliocène supérieur, Rhodes, Grèce), Unpublished MSc, University of Lyon, 2003.

[16] M. Hajjaji, A.-M. Bodergat, P. Moissette, A. Prieur, M. Rio, Signification écologique des associations d'ostracodes de la coupe de Kritika (Pliocène supérieur, Rhodes, Grèce), Rev. Micropaleontol. 41 (1998) 211–233.

[17] B. Keraudren, Les formations quaternaires marines de la Grèce, Bull. Mus. Anthropol. Prehist. Monaco 6 (1970) 5–153.

[18] W. Sissingh, Late Cenozoic Ostracoda of the South Aegean Island Arc, Utrecht Micropaleontol. Bull. 6 (1972) 1–187.

[19] L. Benda, J.E. Meulenkamp, A. van de Weerd, Biostratigraphic correlations in the Eastern Mediterranean Neogene. 3. Correlation between mammal, sporomorph and marine microfossil assemblages from the Upper Cenozoic of Rhodos, Greece, Newsl. Stratigr. 6 (1977) 117–130.

[20] L. Blanc-Vernet, H. Chamley, B. Keraudren, J. Sauvage, A propos de la limite plio-pleistocène dans les séquences marines de l'île de Rhodes (Dodécanèse, Grèce), C. R. Acad. Sci., Ser. D 280 (1975) 541–544.

[21] E. Thomsen, T.L. Rasmussen, A. Hastrup, Calcareous nannofossil, ostracode and foraminifera biostratigraphy of Plio-Pleistocene deposits, Rhodes (Greece), with a correlation to the Vrica section (Italy), J. Micropalaeontol. 20 (2001) 143–154.

[22] T.L. Rasmussen, A. Hastrup, E. Thomsen, Lagoon to deep-water foraminifera and ostracods from the Plio-Pleistocene Kallithea bay section, Rhodes, Greece, in: E. Thomsen (Ed.), Special Publication, vol. 39, Cushman Foundation for Foraminiferal Research, 2005, pp. 1–290.

[23] N. Spjeldnaes, P. Moissette, Celleporid (bryozoan) thickets from the upper Pliocene of the Island of Rhodes, Greece, in: N.P. James, J.A.D. Clarke (Eds.), Cool-water carbonates, SEPM Special Publication, vol. 56, Society of Economic Paleontologists and Mineralogists, Tulsa, 1997, pp. 263–270.
[24] M. Steinthorsdottir, Depositional environment of the Pliocene Kolymbia Limestone, Rhodes, Greece, Unpublished MSc, University of Copenhagen, 2002.
[25] L.J. Beckman, Stratigraphical and sedimentological investigations of Pliocene/Pleistocene deposits at Lindos Bay, Rhodes, Unpublished Ph.D., University of Tromsø, 1995.
[26] R. Løvlie, G. Støle, N. Spjeldnaes, Magnetic polarity stratigraphy of Pliocene–Pleistocene marine sediments from Rhodos, eastern Mediterranean, Phys. Earth Planet. Inter. 54 (1989) 340–352.
[27] J. Titschack, R.G. Bromley, A. Freiwald, Plio-Pleistocene cliff-bound, wedge-shaped, warm-temperate carbonate deposits from Rhodes (Greece): sedimentology and facies, Sediment. Geol. 180 (2005) 29–56.
[28] G. Orombelli, C. Montanari, Geological studies on the Dodecanese islands (Aegean Sea). VI. The Calabrian of the island of Rhodes (Greece), preliminary information, Boll. Soc. Geol. Ital. 86 (1967) 103–113.
[29] D. Frydas, Die Pliozän/Pleistozän-Grenze auf der Insel Rhodos (Griechenland), Munst. Forsch. Geol. Palaontol. 76 (1994) 331–344.
[30] K.S. Hansen, Development of a prograding carbonate wedge during sea level fall: Lower Pleistocene of Rhodes, Greece, Sedimentology 46 (1999) 559–576.
[31] J.A. Broekman, Sedimentation and paleoecology of Pliocene lagoonal-shallow deposits on the island of Rhodos (Greece), Unpublished Ph.D., Rijks Universiteit, Utretch, 1972.
[32] R.A.F. Cas, J.V. Wright (Eds.), Volcanic successions, Modern and Ancient, Unwin Hyman Ltd, 1988, 487 pp.
[33] G.A. Smith, J.E. Lotosky, What factors control the composition of andesitic sands? J. Sediment. Res. A65 (1995) 91–98.
[34] P. Moissette, N. Spjeldnaes, Plio-Pleistocene deep-water bryozoans from Rhodes, Greece, Palaeontology 38 (1995) 771–799.
[35] H. Bellon, J.J. Jarrige, D. Sorel, Les activités magmatiques égéennes de l'Oligocène à nos jours et leurs caractères géodynamiques. Données nouvelles, Rev. Geol. Dyn. Geogr. Phys. 21 (1979) 41–55.
[36] S. Nomade, P.R. Renne, N. Vogel, A.L. Deino, W.D. Sharp, T.A. Becker, A.R. Jaouni, R. Mundil, Alder Creek Sanidine (ACs-2): a Quaternary $^{40}Ar/^{39}Ar$ dating standard tied to the Cobb Mountain geomagnetic event, Chem. Geol. 218 (2005) 315–338.
[37] J.L. Kirschvink, The least-squares line and plane and the analysis of palaeomagnetic data, Geophys. J. R. Astron. Soc. 62 (1980) 699–718.
[38] T.A.T. Mullender, A.J. van Velzen, M.J. Dekkers, Continuous drift correction and separate identification of ferrimagnetic and paramagnetic contribution in thermomagnetic runs, Geophys. J. Int. 114 (1993) 663–672.
[39] A.P. Roberts, C.R. Pike, K.L. Verosub, First-order reversal curve diagrams: a new tool for characterising the magnetic properties of natural samples, J. Geophys. Res. 102 (2000) 28461–28475.
[40] C.R. Pike, A.P. Roberts, K.L. Verosub, First-order reversal curve diagrams and thermal relaxation effects in magnetic particles, Geophys. J. Int. 145 (2001) 721–730.
[41] J.P. Kennett, M.S. Srinivasan (Eds.), Neogene planktonic foraminifera: a phylogenetic atlas, Hutchinson Ross Publishing Company, Stroudsburg, Pennsylvania, 1983, 230 pp.
[42] D.J. Dunlop, Ö. Özdemir, Rock Magnetism: Fundamentals and Frontiers, Cambridge University Press, Cambridge, 1997 573 pp.
[43] W.A. Berggren, F.J. Hilgen, C.G. Langereis, D.V. Kent, J.D. Obradovich, I. Raffi, M.E. Raymo, N.J. Shackleton, Late Neogene chronology: new perspectives in high-resolution stratigraphy, GSA Bull. 107 (1995) 1272–1287.
[44] L.J. Lourens, F.J. Hilgen, J. Laskar, N.J. Shackleton, D.S. Wilson, The Neogene period, in: F.M. Gradstein, J.G. Ogg, A.G. Smith (Eds.), A Geologic Time Scale 2004, Cambridge University Press, Cambridge, 2005, pp. 409–440.
[45] J.E.T. Channel, D. Rio, R. Sprovieri, G. Glaçon, in: K.A. Kasten, J. Mascle (Eds.), Biomagnetostratigraphic correlations from Leg 107 in the Tyrrhenian Sea, Proceedings of the Ocean Drilling Program, Scientific Results, vol. 107, 1990, pp. 669–682.
[46] J.D.A. Zijderveld, F.A. Hilgen, C.G. Langereis, P.J.J.M. Verhallen, W.J. Zachariasse, Integrated magnetostratigraphy and biostratigraphy of the upper Pliocene–lower Pleistocene from the Monte Singa and Crotone areas in Calabria, Italy, Earth Planet. Sci. Lett. 107 (1991) 697–714.
[47] G.M. DiPaola, Volcanology and petrology of Nisyros Island Dodecanese, Greece, Bull. Volcanol. 38 (1974) 944–987.
[48] M. Fytikas, O. Giuliani, F. Innocenti, G. Marinelli, R. Mazzuoli, Geochronological data on Recent magmatism of the Aegean Sea, Tectonophysics 31 (1976) T29–T34.
[49] H. Bellon, J.J. Jarrige, L'activité magmatique néogène et quaternaire dans l'ile de Kos, Grèce: Données radiochronologiques, C. R. Acad. Sci. Paris 288 (1979) 1359–1362.
[50] S.R. Allen, Reconstruction of a major caldera-forming eruption from pyroclastic deposit characteristics: Kos Plateau Tuff, eastern Aegean Sea, J. Volcanol. Geotherm. Res. 105 (2001) 141–162.
[51] A. Buettner, I.C. Kleinhanns, D. Rufer, J.C. Hunziker, I.M. Villa, Magma generation at the easternmost section of the Hellenic arc: Hf, Nd, Pb and Sr isotope geochemistry of Nisyros and Yali volcanoes (Greece), Lithos 83 (2005) 29–46.
[52] E. Kovacs, N. Spjeldnaes, Pliocene–Pleistocene stratigraphy of Rhodes, Greece, Newsl. Stratigr. 37 (1999) 191–208.
[53] J. Woodside, J. Mascle, C. Huguen, A. Volkonskaia, The Rhodes Basin, a post-Miocene tectonic trough, Mar. Geol. 165 (2000) 1–12.
[54] C. Kissel, C. Laj, The Tertiary geodynamic evolution of the Aegean arc: a paleomagnetic reconstruction, Tectonophysics 146 (1988) 183–201.
[55] C. Kissel, C. Laj, A. Poisson, G.N., Paleomagnetic reconstruction of the Cenozoic evolution of the Eastern Mediterranean, Tectonophysics 362 (2003) 199–217.
[56] D.J.J. van Hinsbergen, C.G. Langereis, J.E. Meulenkamp, Revision of the timing, magnitude and distribution of Neogene rotations in the western Aegean region, Tectonophysics 396 (2005) 1–34.
[57] C.E. Duermeijer, W. Krijgsman, C.G. Langereis, J.E. Meulenkamp, M.V. Triantaphyllou, W.J. Zachariasse, A late Pleistocene clockwise rotation phase of Zakynthos (Greece) and implications for the evolution of the western Aegean arc, Earth Planet. Sci. Lett. 173 (1999) 315–331.
[58] C.E. Duermeijer, W. Krijgsman, C.G. Langereis, J.H. Ten Veen, Post–early Messinian counterclockwise rotations on Crete: implications for Late Miocene to Recent kinematics of the southern Hellenic arc, Tectonophysics 298 (1998) 177–189.